A novel mouse model of non-alcoholic steatohepatitis suggests that liver fibrosis initiates around lipid-laden macrophages

Running title: Liver fibrosis begins around macrophages

Mayuko Ichimura-Shimizu[1,2], Yosuke Tsuchiyama[1], Yuki Morimoto[1], Minoru Matsumoto[3], Tomoko Kobayashi[1], Satoshi Sumida[1], Takumi Kakimoto[1], Takeshi Oya[3], Hirohisa Ogawa[1], Michiko Yamashita[4], Satoru Matsuda[2], Katsuhisa Omagari[5], Shu Taira[6], Koichi Tsuneyama[1,3]

[1] Department of Pathology and Laboratory Medicine, Institute of Biomedical Sciences, Tokushima University Graduate School, Tokushima, Japan

[2] Department of Food Science and Nutrition, Nara Women's University, Kita-Uoya Nishimachi, Nara, Japan

[3] Department of Molecular Medicine, Institute of Biomedical Sciences, Tokushima University Graduate School, Tokushima, Japan

[4] Morphological Laboratory Science, Institute of Biomedical Sciences, Tokushima University Graduate School, Tokushima, Japan

[5] Division of Nutritional Science, Graduate School of Human Health Science, University of Nagasaki, Nagasaki, Japan

[6] Faculty of Food and Agricultural Sciences, Fukushima University, Kanayagawa, Fukushima,

Japan

Address correspondence and reprint requests to Koichi Tsuneyama, MD, PhD, Department of Pathology and Laboratory Medicine, Graduate School of Biomedical Sciences, Tokushima University, Kuramoto, Tokushima 770-8503, Japan Tel: +81-88-633-7065 Fax: +81-88-633-7067

E-mail: tsuneyama.koichi@tokushima-u.ac.jp

Financial support:

This work was supported by JSPS KAKENHI Grant-in-Aid for Scientific Research (A) No. 17H00881 and (C) No. 18K07069 (to K.T) and for Young Scientists No. 20K19676 (to M.I-S).

Disclosure of conflict of interest

The authors declare that they have no conflicts of interest.

Number of text pages: 26; number of tables: 4; number of figures: 5

Abstract

Various cells such as macrophages and hepatic stellate cells interact in the generation of fibrosis in nonalcoholic steatohepatitis (NASH), but the mechanism remains unclear. We employed a high fat/cholesterol/cholate (HFCC) diet to generate a model of NASH-related fibrosis and investigate the pathogenesis of fibrosis. Two mouse strains differing in susceptibility to obesity, the susceptible strain C57BL/6J (B6) and the relatively resistant strain A/J, developed hepatic histological features of NASH including fat deposition, intralobular inflammation, hepatocyte ballooning, and fibrosis after 9 weeks of HFCC diet feeding. The severity of hepatic inflammation and fibrosis was greater in A/J mice than in B6 mice. A/J mice fed the HFCC diet exhibited characteristic CD204-positive lipid-laden macrophage aggregation in hepatic parenchyma. Polarized light visualized the Maltese cross, namely cholesterol crystals within the aggregated macrophages. Moreover, fibrosis developed in a ring-shape from the periphery of the aggregated macrophages, i.e., the starting point of fibrosis could be visualized histologically. Furthermore, matrix assisted laser desorption/ionization mass spectrometry imaging analysis detected a molecule at *m/z* 772.462, which corresponds to the protonated ion of phosphatidylcholine (P-18:1 (11Z)/18:0) and phosphatidylethanolamine (18:0/20:2 (11Z, 14Z)), in aggregated macrophages in adjacent to the fibrotic lesions. In conclusion, the present HFCC diet-fed A/J model provides an ideal tool to study fibrogenesis and enables novel insights into the pathophysiology of NASH-related fibrosis.

Introduction

The number of people experiencing metabolic syndrome manifesting as obesity, high blood pressure, diabetes, dyslipidemia and non-alcoholic fatty liver disease (NAFLD)/non-alcoholic steatohepatitis (NASH), has been rapidly increasing worldwide in recent years [1, 2, 3]. NASH is a more severe form of NAFLD, which involves parenchymal inflammation and perivenular/pericellular fibrosis [4, 5]. Unlike viral hepatitis with noteworthy necrosis of hepatocytes, NASH fibrosis is characterized by elongation of fine fibers surrounding living hepatocytes [6]. During the process of regeneration and tissue repair, granulation tissue occurs as the first step, and extracellular matrix including collagen fibers is gradually deposited in the granulation tissue. Various inflammatory cells, as well as epithelial cells and mesenchymal cells, migrate and cooperate during regeneration and tissue repair. Fibrosis eventually subsides with successful tissue repair; however, fibrosis is thought to progress when tissue repair is incomplete. The interaction of macrophages and hepatic stellate cells is known to be a key event of fibrogenesis in the liver [7, 8, 9, 10, 11]. Fibrogenesis is strictly controlled by complex crosstalk between these cells through production of various growth factors and cytokines, such as transforming growth factor (TGF)-β and platelet-derived growth factor (PDGF)-β.

Studies on these fibrotic processes have been conducted mainly in patients with viral hepatitis and mouse models induced by carbon tetrachloride [12, 13]. However, questions remain regarding the mechanism of fibrosis progression in NASH, as there have been few mouse models replicating the pericellular fibrosis characteristics of NASH. Fibrosis occurs in a complex manner;

76 therefore, a mouse model capable of reproducing the fibrosis process of human NASH is required.
77 Previous studies reported a model of NASH-related cirrhosis mimicking the human fibrotic
78 pattern of NASH in rats fed a high fat/cholesterol/cholate (HFCC) diet [14, 15]. We also applied this
79 diet to various mouse strains and revealed that the severity and pattern of liver fibrosis differed
80 significantly among strains. In the preliminary study using A/J mice, which are known to be
81 resistance to diet-induced obesity [16 17, 18], those fed the HFCC diet developed liver histology that
82 is similar to human NASH. Additionally, the aggregation of lipid-laden macrophages in liver
83 parenchyma and ring-shaped fibrous extensions around them were observed. The link between
84 macrophage aggregation and the onset of fibrosis made it possible to capture the onset of fibrosis
85 histologically in this mouse model. As a result, matrix assisted laser desorption/ionization mass
86 spectrometry imaging (MALDI-MSI) analysis indicated that specific phospholipids were
87 localized in macrophages associated with fibrosis. Thus, the HFCC diet-fed A/J mice might
88 provide novel insights into the pathophysiology of NASH-related fibrosis.
89
90 **Materials and Methods**
91 *Animal model and experimental design*
92 Eight-week-old male C57BL6/J (B6) mice and 8-week-old male A/J mice were
93 purchased from Japan SLC (Hamamatsu, Japan) and housed individually in a temperature- and
94 humidity-controlled room with a 12-h light/dark cycle. Since there are sex differences in the
95 severity of fatty degeneration and inflammation, and female mice are more resistant to their

development, only male mice were used in this study to create an advanced NASH model. [19 20] After 1 week of acclimation with standard rodent chow (MF; Oriental Yeast, Tokyo, Japan), the two strains of mice were each randomly divided into 3 groups: Normal diet group (N group) fed standard chow (MF), low-dose cholesterol (LC) diet group fed iHFC #5-based diet (69.5% MF, 28.75% palm oil, 0.5% cholate) with 1.25% cholesterol, and high-dose cholesterol (HC) diet group fed iHFC #5-based diet (69.5% MF, 27.5% palm oil, 0.5% cholate) with 2.5% cholesterol. The iHFC diet is high in fat, cholesterol and cholate, and can induce NASH-related fibrosis[21] (Hayashi Kasei, Osaka, Japan). The number of mice in the B6-N, B6-LC, B6-HC, A/J-N, A/J-LC and A/J-HC groups was 5, 6, 4, 5, 5 and 5, respectively. All mice had free access to food and water. Daily energy intake and body weight were monitored throughout the study.

At 18 weeks of age, the mice were euthanized under anesthesia with isoflurane. Blood was collected from the inferior vena cava, and the resulting serum samples were kept at −20°C. The epididymal fat pad and liver were removed and weighed. The liver tissue was fixed in 10% neutral-buffered formalin or immediately frozen in liquid nitrogen and stored at −80°C. All animal experimentation procedures were approved by the Animal Use Committee of Nara Women's University, and the animals were maintained in accordance with the guidelines for the care and use of laboratory animals, Nara Women's University.

Serum and tissue biochemical analyses

Hepatic lipids were extracted as described previously [14]. Serum and/or tissue levels of

116 triglyceride (TG), total cholesterol (TC), glucose, alanine aminotransferase (ALT) and aspartate
117 aminotransferase (AST) were determined using Triglyceride E test Wako, Cholesterol E test Wako,
118 Glucose C II test Wako, and Transaminase C II test Wako, respectively (Fujifilm Wako Pure
119 Chemical, Osaka, Japan). Insulin and leptin levels were measured using a mouse insulin enzyme-
120 linked immunosorbent assay (ELISA) kit and a leptin ELISA kit (Morinaga Institute of Biological
121 Science, Yokohama, Japan). Serum levels of TG and cholesterol in each lipoproteins including
122 very low density lipoprotein (VLDL), low density lipoprotein (LDL) and high density lipoprotein
123 (HDL) were measured by the LipoSEARCH service (Skylight Biotech Inc., Akita, Japan) using
124 gel-filtration high performance liquid chromatography.
125
126 *Histopathological analysis*
127 Liver tissues were fixed in 10% phosphate-buffered formalin, embedded in paraffin,
128 sectioned at 2 μm thickness and stained with hematoxylin and eosin (H&E) and Sirius red
129 according to standard procedures. Histological steatosis (0 to 3), lobular inflammation (0 to 3)
130 and hepatocyte ballooning (0 to 2) were assessed semi-quantitatively to determine the NAFLD
131 activity score (NAS) according to the criteria proposed by Kleiner et al [22]. NAS scores ≥ 5 and $\leq$
132 2 were considered diagnostic and not diagnostic, respectively, for steatohepatitis. Liver fibrosis
133 (0 to 4) was also assessed according to this system. To detect lipid accumulation, a frozen
134 specimen of the liver was sliced to a thickness of 5 μm and the presence of crystal structures was
135 observed using polarized light microscopy and stained with oil red O. All histopathological

136 findings were evaluated by several pathologists in a blinded manner.

137 Liver tissues were immunostained for Mac2, CD204, monocyte chemotactic protein
138 (MCP)-1 and PDGF-receptor β (PDGF-Rβ) to characterize the cell group that constitutes the
139 microenvironment surrounding macrophages. Paraffin-embedded and frozen sections were
140 incubated with anti-CD204 (1:200, Bioss Inc., Woburn, MA, USA), anti-type I collagen (1:200,
141 Rockland Immunochemicals, PA, USA), anti-type IV collagen (1:100, Merck Millipore,
142 Darmstadt, Germany), anti-MCP-1 (1:100, Bioss), anti-Mac2 (1:100; Cedarlane, Burlington, ON,
143 Canada) and anti-PDGF-Rβ (1:50; Cell Signaling, Beverly, MA, USA). For the subsequent
144 reactions, Envision-PO for rabbit polyclonal antibodies (Dako, Glostrup, Denmark) and Simple
145 stain mouse MAX-PO (Nichirei Bioscience, Tokyo, Japan) were used as the secondary antibody,
146 and 3,3'-diaminobenzidine (Dako) was used for color development.

147

148 *MALDI-MSI analysis*

149 Liver tissues were embedded in 4% carboxymethyl cellulose, snap-frozen, sectioned at
150 5-μm thickness and mounted onto indium tin oxide-coated slides (Bruker Daltonics, Billerica,
151 MA, USA). Optical images of the sections were obtained using a scanner (GTX830; Epson, Tokyo,
152 Japan) before analysis by MALDI-MSI. The matrix solution was prepared using 40 mg of α-
153 cyano-4-hydroxycinnamic acid (Nacalai Tesque, Kyoto, Japan) in 6 ml of
154 acetonitrile/water/trifluoroacetic acid: 70/29.9/0.1 (v/v) and sprayed onto tissue sections using an
155 automated pneumatic sprayer (TM-Sprayer; HTX Tech., Chapel Hill, NC, USA). Ionization and

156 imaging of phospholipids were confirmed with matrix-assisted laser desorption/ionization time-
157 of-flight mass spectrometry (MALDI-TOF-MS, rapifleX; Bruker Daltonics). The spatial
158 resolution for the imaging data was 20 μm. Software from Bruker Daltonics (FlexImaging version
159 5.0) was used for the data analysis. Candidate lipids were identified using lipid databases such as
160 LIPIDMAPS (https://www.lipidmaps.org/; last accessed May 8th, 2020). Finally, tandem MS
161 (MS/MS) analysis was performed to confirm the chemical structure of lipids. The adjacent section
162 stained with H&E was used to recognize the location of aggregated macrophages in heat map
163 images of MALDI-MSI.
164
165 *Gene expression analysis in liver*
166 Total RNA from the liver was prepared using RNAiso Plus (Takara Bio, Otsu, Japan),
167 and cDNA was synthesized using ReverTra Ace qPCR RT Master Mix (Toyobo, Osaka, Japan)
168 according to the manufacturer's instructions. SYBR Green real-time PCR was performed using
169 THUNDERBIRD SYBR qPCR Mix (Toyobo), specific primers (Table 1) and a LightCycler Nano
170 (Roche, Basel, Switzerland). All quantifications were normalized to β-actin. Data were
171 determined using the $2^{-\Delta\Delta Ct}$ method and expressed as relative expression to that of the B6-N group.
172
173 *Western blot*
174 Liver tissues were homogenized mechanically and subsequently lysed on ice in RIPA
175 buffer (Nakalai tesque) with protease inhibitor. Homogenates were then centrifuged at 10,000*g*

for 20 min at 4°C, and supernatants collected. Ten μg of protein was subjected to polyacrylamide gel electrophoresis (7.5% or 12%) followed by electroblotting onto a nitrocellulose membrane (GE Cytiva, Tokyo, Japan). To detect the immunocomplex, an Immobilon HRP substrate (Merck Millipore) and Chemiluminescence Imaging System (FUSION SOLO,7S,EDGE; Vilber, Marne-la-Vallée, France) were used. Primary antibodies for immunoblot analysis were used at dilutions of 1:1000 for fatty acid synthase (FASN; Abcam, Cambridge, UK) and 1:10000 for β-actin (Merck Millipore). The images were converted to TIFF files and analyzed using NIH ImageJ software (version 1.53k, https://imagej.nih.gov/ij/; last accessed September 27th, 2021).

Statistical analysis

Data are presented as means ± standard error (SE). Group means analyzed by two-way analysis of variance (ANOVA), followed by Tukey's *post hoc* test when a significant interaction between factors (i.e., strain and diet) was determined. In the absence of such interaction and the presence of significant effects by either strain or diet, differences between groups were analyzed by a t-test or Tukey's test, respectively. A P value of less than 0.05 was considered to be statistically significant. Analyses were performed with GraphPad Prism 7.02 (GraphPad Software, San Diego, CA, USA).

Results

196 *Cumulative energy intake, body weight and relative organ weights*

197 After 9 weeks of feeding, the cumulative energy intake and body weight gain compared
198 to baseline did not differ significantly among the groups (Table 2). The final body weight was
199 significantly higher in the B6-LC group compared to the A/J-LC group. The liver and spleen
200 weight/body weight ratios were dose-dependently higher in the mice fed the LC and HC diets.
201 The liver weight/body weight ratio was also higher in the A/J-LC and A/J-HC groups than in the
202 B6-LC and B6-HC groups, respectively. There was no significant difference in the epididymal fat
203 pad weight/body weight ratio among the groups.

204

205 *Serum biochemical parameters and hepatic lipid concentrations*

206 Hepatic TG content was dose-dependently higher, but serum TG levels were
207 significantly lower in the A/J-LC and A/J-HC groups (Figure 1A) than in the A/J-N group (Figure
208 1B). There were no significant differences in serum and hepatic TG levels among the B6 strain
209 groups (Figure 1A, B). The serum levels of VLDL-TG, a lipid excreted from the liver, decreased
210 with the HFCC diet intake and were lower in A/J-HC group than B6-HC group (Figure 1C).
211 Consistent with serum VLDL-TG levels, mRNA levels of apolipoprotein B (ApoB), a constituent
212 of VLDL, were dose-dependently decreased in the HFCC diet-fed groups (Figure 1D). Hepatic
213 and serum TC levels and serum LDL-C levels of the mice fed LC and HC diets were higher than
214 those fed the normal diet in both strains (Figure 1E, F and Table 3). Furthermore, A/J mice fed
215 the LC and HC diets showed significantly higher hepatic cholesterol content compared with the

B6 mice (Figure 1E). Serum ALT levels were increased by HC diet feeding only in the A/J mice (Figure 1G). Serum AST levels tended to be higher in dependent on cholesterol intake in both strain, although there were no significant differences among groups. AST/ALT ratio tended to be dose-dependently lower in the HFCC diet-fed groups (Table 3). The serum glucose, insulin, leptin and HDL-C levels did not differ significantly among the groups.

Liver histopathology

Figure 2A and Table 4 show representative liver images and histological assessments of mice, respectively. No individuals with fat deposition, inflammation, or fibrosis were found in the B6-N and A/J-N groups. Fatty changes localized around the central vein (zone 3-2), lobular inflammation and ballooning hepatocytes were observed in both strains fed LC and HC diets, and these observations were more severe in A/J mice than B6 mice. Mild to moderate steatosis (grade 1 or 2) was observed in all 5 mice in the A/J-LC and A/J-HC groups, 4 (66%) of 6 mice in the B6-LC group and all 4 mice in the B6-HC group (Table 3). In addition, the severity of fatty change was dependent on the amount of cholesterol intake only in the A/J strain. Oil red O staining indicated deposition of small lipid droplets that could not be found in H&E staining (Figure 2A). According to NAS, 4 (80%) of 5 mice in both the A/J-LC and A/J-HC groups, 2 (33%) of 6 mice in the B6-LC group and 1 (20%) of 5 mice in the B6-HC group were diagnosed with NASH (i.e., having a NAS of 5 or greater). Collagen fiber was identified by Sirius red staining of LC and HC groups in both the B6 mice and A/J mice (Figure 2A, B). Mild fibrosis (stage 1-2) was observed

236 in all 5 mice in the A/J-LC and A/J-HC groups, all 6 mice in the B6-LC group and 3 (60%) of 5
237 mice in the B6-HC group. All 6 mice in the B6-LC group, 2 (50%) of 4 mice in the B6-HC group,
238 4 (80%) of 5 mice in the A/J-LC group, and 2 (40%) of 5 mice in the A/J-HC group had very
239 slight fibrosis (stage 1). Meanwhile, 1 (25%) of 4 mice in the B6-HC group, 1 (20%) of 5 mice in
240 the A/J-LC group and 3 (60%) of 5 mice in the A/J-HC group showed moderate fibrosis around
241 the portal area as well as the perisinusoidal area (stage 2). In addition to the typical NASH findings,
242 a unique and characteristic lesion was observed in mice fed the HFCC diet, which was more
243 frequent in the A/J strain. Figure 2C-K shows the hepatic parenchyma of the A/J-HC group in
244 higher magnification. Aggregates of foamy cells resembled small cell nests and were dispersed
245 throughout the tissue (Figure 2C). Sirius red staining revealed that these unique structures were
246 surrounded by slender and delicate collagen fibers (Figure 2D). Collagen type I and IV was also
247 deposited around these structures (Figure 2E, F). We named this unique fibrosis pattern “ring-
248 shaped fibrosis”. To characterize aggregated foamy cells, immunostaining was performed using
249 the macrophage markers Mac-2 and CD204 (Figure 2G, H). As expected, aggregated cells
250 surrounded by ring-shaped fibrosis were foamy macrophage clusters. In addition, using polarized
251 light microscopy, Maltese crosses, spherical crystals of cholesterol [23], were observed in
252 aggregated foamy macrophages in the same frozen section before immunostaining with H&E
253 (Figure 2I). Next, immunostaining was performed with the hepatic stellate cell markers MCP-1
254 and PDGF-Rβ. Interestingly, MCP-1 positive mononuclear cells were proximally located to the
255 foamy cell nests (Figure 2J). In addition, PDGF-Rβ showed ring-shaped staining surrounding the

256 foamy cell nests (Figure 2K). These findings suggested that MCP-1-positive cells transformed to
257 PDGF-Rβ-positive spindle cells, namely active myofibroblasts, and generated collagen fibers. In
258 contrast, B6 mice fed the HC diet showed cholesterol crystals and surrounding macrophages, but
259 less aggregation of macrophages and ring-shaped fibrosis in the liver (Supplemental Figure S1).
260
261 *MALDI-MSI analysis of liver*
262 To characterize the lipids in foamy macrophage nests, MALDI-MSI analysis was
263 performed in positive-ion mode. In the liver sections obtained from A/J-HC mice, a protonated
264 molecular ($[M+H]^+$) ion at *m/z* 772.462 was observed in conformity with the location of
265 aggregated macrophage nests (Figure 3A), although most of the molecular ions were diffusely
266 distributed similar to the ion at *m/z* 369.6 (Supplemental Figure S2). To determine the structure
267 of the molecular ion at *m/z* 772.462, MS/MS analysis was performed in positive- and negative-
268 ion mode. The product ions included a $[M+H]^+$ ion at *m/z* 184.063 and a $[M+H]^+$ ion at *m/z* 156.0,
269 which represent choline and ethanolamine as head groups of phospholipids, respectively (Figure
270 3C). Together with the other product ions (Figure 3D), the $[M+H]^+$ ion at *m/z* 772.462 was
271 surmised to be phosphatidylcholine (P-18:1 (11Z)/18:0) or phosphatidylethanolamine (18:0/20:2
272 (11Z, 14Z)) using the comprehensive lipid database LIPIDMAPS.
273
274 *Gene and protein expression in liver*
275 Consistent with the histological fibrosis observations in the liver, the expression levels

276 of mRNAs encoding procollagen type I, alpha 1 (Col1a1), procollagen type IV, alpha 1 (Col4a1)
277 and Tgf-β1 were dose-dependently higher in the HFCC diet-fed groups (Figure 4A-C). The
278 mRNA levels of pro-inflammatory cytokines such as tumor necrosis factor-α (Tnf-α) were dose-
279 dependently higher in the HFCC diet-fed groups and were higher in A/J mice than B6 mice
280 (Figure 4D), although there were no significant differences among groups in the mRNA levels of
281 interleukin-6 (Il-6) and p65 (Supplemental Figure S3). Next, genes and protein involved in lipid
282 metabolism were analyzed. The mRNA levels of sterol regulatory element-binding protein-1c
283 (Srebp-1c), which was involved in de novo lipogenesis, did not differ significantly among the
284 groups (Figure 4E), while the relative expression of FASN protein, a rate-limiting enzyme of
285 lipogenesis, decreased in HFCC diet-fed groups and was lower in A/J-N than B6-N group and in
286 A/J-HC than B6-HC group, respectively (Figure 4F). The mRNA levels of long-chain acyl-CoA
287 synthase 1 (Acsl1), which is an essential enzymes that activate fatty acids as a substrate for TG,
288 were lower in the HFCC diet-fed groups (Figure 4G). The mRNA levels of apolipoprotein C3
289 (ApoC3), which is a constituent of VLDL and HDL and inhibiting lipoprotein lipase (LPL), were
290 lower in the HFCC diet-fed groups (Figure 4H). Next, key molecular markers of cholesterol
291 metabolism including biosynthesis, uptake, efflux, and conversion to bile acid were analyzed;
292 however, cholesterol accumulation in the liver of A/J strain feeding HFCC diet could not be
293 explained at the mRNA level (Supplemental Figure S3).
294
295 **Discussion**

296 The present study showed that feeding the HFCC diet induced hepatic histological
297 features of NASH, including fat deposition, intralobular inflammation, hepatocyte balloon-like
298 swelling, and fibrosis, in both obesity-prone B6 mice and obesity-resistant A/J mice. The severity
299 of NASH-like lesions and fibrosis was greater in A/J mice than in B6 mice. Interestingly, A/J mice
300 showed characteristic lipid-laden macrophage aggregation in the hepatic parenchyma, and
301 fibrosis development showed a ring shape from the periphery of macrophage aggregation.
302 Although these unique histological findings may be specific to mouse fibrosis, the A/J strain fed
303 the HFCC diet is a useful model for visualizing the "starting point" of liver fibrosis in NASH,
304 since few NASH-related fibrosis models are available [24].

305 Accumulating evidence indicates that macrophages and hepatic stellate cells interact
306 with each other in the progression of liver fibrosis [7-11]. However, it has been difficult to visualize
307 the direct interaction of these cells at the initiation of fibrosis. In the present study, HFCC diet
308 feeding to A/J mice allowed visualization of the hepatic microenvironment, including initial
309 fibrosis extension around the aggregated macrophages. As expected, MCP-1-positive activated
310 hepatic stellate cells were located at the periphery of foamy macrophage nests and PDGF-Rβ-
311 positive spindle cells also surrounded the foamy macrophage nests (Figure 5). The reason for
312 choosing the HFCC diet was that the composition was designed to accelerate fibrosis in NASH[21].
313 We have previously confirmed that this diet induced stage 3 fibrosis with macrophage infiltration
314 in Tsumura-Suzuki non-obese strain, however, the aggregation of multiple macrophages was less
315 as well as C57BL6/J strain (unpublished data). Taken together, HFCC diet-fed A/J mice might

316 provide important information regarding fibrogenesis.

317 The excessive hepatic accumulation of lipids and activation of macrophages in response
318 to these stimuli are implicated in the development and progression of NASH [25]. In the present
319 study, the aggregated foamy macrophages observed in A/J mice fed the HFCC diet were
320 considered to be CD204-positive M2 macrophages. Some crystals, characterized by the Maltese
321 cross, were contained in the cytoplasm of these macrophages and were considered to be lipids,
322 since it is known that cholesterol crystals are commonly observed in the liver of NASH patients
323 and animals [23 26] as well as in atherosclerotic lesions [27]. The remarkable increase in hepatic Tnf-α
324 mainly produced by macrophages also supported the link between cholesterol and macrophage
325 activation, especially in A/J mice. Then, the cytokines from activated macrophages might
326 stimulate other cells including fibroblasts, leading to an increase in fibrosis markers such as
327 collagen and Tgf-β1. In addition, MALDI-MSI analysis showed that *m/z* 772.462, which
328 corresponds to the $[M+H]^+$ ion of phosphatidylcholine (P-18:1 (11Z)/18:0) or
329 phosphatidylethanolamine (18:0/20:2 (11Z, 14Z)), was located in aggregated foamy macrophages.
330 Recent studies revealed that macrophage metabolism, including upregulated fatty acid synthesis,
331 changes dynamically in the inflammatory response [28, 29]. In addition, some phospholipids are
332 involved in promoting liver regeneration [30 31]. Further studies are needed for detailed
333 characterization of the effects of these phospholipids on the progression of liver fibrosis.

334 Diets containing high-fat and cholesterol have been reported to play an important role
335 in the dysregulation of lipid metabolism[14 32]. In the present study, the HFCC diet decreased TG

336 clearance from the liver, as indicated by low levels of VLDL-TG and ApoB, resulting in hepatic
337 lipid accumulation. The low serum TG levels in HFCC-fed mice despite high fat intake may be
338 partly due to the low release of VLDL-TG as well as the reduced expression of ApoC3, an
339 inhibitor of LPL, which catalyzes the hydrolysis of lipoprotein TG. The HFCC diet also reduced
340 FASN expression, consistent with previous studies [14] [15]. It is possible that excessive lipid
341 accumulation may cause negative feedback regulation of FASN in the liver, although the reason
342 for the discrepancy between expression of FASN and Srebp1c, a transcription factor involved in
343 lipogenesis, was unclear. Further investigation such as whole-transcriptomic analysis will help
344 clarify the mechanism by which NASH develops in mice fed the HFCC diet.

345 It is known that the severity of NASH and fibrosis is greater in diabetes patients [33] [34].
346 The HFCC diet-fed mice showed NASH with high levels of serum ALT in the A/J strain only. The
347 diet also induced hepatic cholesterol accumulation, abnormal lipoprotein metabolism and an
348 increase in inflammatory cytokines seen in human NASH [35-37], although there were no significant
349 changes in body weight and serum levels of glucose, insulin and leptin. These results suggest that
350 the HFCC diet causes dysregulation of lipid metabolism and hepatic inflammation even in the
351 absence of obesity. This is in contrast to the report by Farrell *et al*., in which NASH did not occur
352 in non-diabetic mice [38]. The contribution of cholate via downregulation of Acsl1 levels may be
353 one of the causes of obesity suppression [39]. Hepatic cholesterol accumulation also has been known
354 to be a critical factor in the development of hepatic steatosis and the progression to steatohepatitis
355 in animal models and NASH patients [40] [32] [41, 42]. Yasutake et al. reported that non-obese NAFLD

356 patients had significantly higher cholesterol intake than obese NAFLD patients [43]. Several reports
357 have shown that about one-third of NAFLD patients are non-obese, especially in the Asian region
358 [2 4, 44] The A/J model of non-obese NASH in this study not only serves as a useful fibrosis model
359 but also demonstrates that caution is warranted in the consumption of high-fat and cholesterol in
360 non-obese individuals.
361

362 **Acknowledgments**

363 The authors would like to thank Takaaki Tsunematsu, Megumi Kume and Yosuke Tominaga,
364 Tokushima University (Tokushima, Japan), for the technical support of biochemistry and
365 histology experiment, and Yuki Hirao, Shiori Yada and Aya Masuoka, Nara Women's University
366 (Nara, Japan), for assistance with the animal breeding and biochemical measurements. The
367 western blot were performed at the Support Center for Advanced Medical Sciences, Tokushima
368 University Graduate School of Biomedical Sciences.
369

370 **Author Contributions**

371 M.I-S., M.S., K.O., and K.T. designed the research and secured funding; M.I-S., Y.T., Y. M., M.M.,
372 T.K., S.S., T.K., K.O., and S.T. performed the experiments; M.I-S., T.O., H.O., M.Y., M.S., and
373 K.T. performed data validation and analysis; and M.I-S. and K.T. prepared the original draft of
374 the manuscript. All authors read and approved the manuscript.
375

376 **References**

377 [1] Michelotti GA, Machado MV, Diehl AM: NAFLD, NASH and liver cancer. Nat Rev
378 Gastroenterol Hepatol 2013, 10:656-65.

379 [2] Wong RJ: Obesity and non-alcoholic fatty liver disease: Disparate associations among Asian
380 populations. World J Hepatol 2014, 6:263.

381 [3] Masarone M, Federico A, Abenavoli L, Loguercio C, Persico M: Non alcoholic fatty liver:
382 epidemiology and natural history. Rev Recent Clin Trials 2014, 9:126-33.

383 [4] Hardy T, Oakley F, Anstee QM, Day CP: Nonalcoholic Fatty Liver Disease: Pathogenesis and
384 Disease Spectrum. Annual Review of Pathology: Mechanisms of Disease 2016, 11:451-96.

385 [5] Koch LK, Yeh MM: Nonalcoholic fatty liver disease (NAFLD): Diagnosis, pitfalls, and
386 staging. Ann Diagn Pathol 2018, 37:83-90.

387 [6] Altamirano-Barrera A, Barranco-Fragoso B, Mendez-Sanchez N: Management strategies for
388 liver fibrosis. Ann Hepatol 2017, 16:48-56.

389 [7] Seki E, Schwabe RF: Hepatic inflammation and fibrosis: Functional links and key pathways.
390 Hepatology 2015, 61:1066-79.

391 [8] Elpek GÖ: Cellular and molecular mechanisms in the pathogenesis of liver fibrosis: An update.
392 World J Gastroenterol 2014, 20:7260.

393 [9] Ramachandran P, Iredale JP: Macrophages: Central regulators of hepatic fibrogenesis and
394 fibrosis resolution. J Hepatol 2012, 56:1417-9.

395 [10] Miura K, Yang L, van Rooijen N, Ohnishi H, Seki E: Hepatic recruitment of macrophages

promotes nonalcoholic steatohepatitis through CCR2. Am J Physiol Gastrointest Liver Physiol 2012, 302:G1310-21.

[11] Xu J, Liu X, Koyama Y, Wang P, Lan T, Kim I-G, Kim IH, Ma H-Y, Kisseleva T: The types of hepatic myofibroblasts contributing to liver fibrosis of different etiologies. Front Pharmacol 2014, 5.

[12] Ma P-F, Gao C-C, Yi J, Zhao J-L, Liang S-Q, Zhao Y, Ye Y-C, Bai J, Zheng Q-J, Dou K-F, Han H, Qin H-Y: Cytotherapy with M1-polarized macrophages ameliorates liver fibrosis by modulating immune microenvironment in mice. J Hepatol 2017, 67:770-9.

[13] Bility MT, Nio K, Li F, McGivern DR, Lemon SM, Feeney ER, Chung RT, Su L: Chronic hepatitis C infection–induced liver fibrogenesis is associated with M2 macrophage activation. Sci Rep 2016, 6:39520.

[14] Ichimura M, Kawase M, Masuzumi M, Sakaki M, Nagata Y, Tanaka K, Suruga K, Tamaru S, Kato S, Tsuneyama K, Omagari K: High-fat and high-cholesterol diet rapidly induces non-alcoholic steatohepatitis with advanced fibrosis in Sprague-Dawley rats. Hepatol Res 2015, 45:458-69.

[15] Ichimura M, Masuzumi M, Kawase M, Sakaki M, Tamaru S, Nagata Y, Tanaka K, Suruga K, Tsuneyama K, Matsuda S, Omagari K: A diet-induced Sprague–Dawley rat model of nonalcoholic steatohepatitis-related cirrhosis. J Nutr Biochem 2017, 40:62-9.

[16] Catherine Gallou-Kabani AV, Marie-Sylvie Gross, Jean-Pierre Rabès, Catherine Boileau, Christiane Larue-Achagiotis, Daniel Tomé, Jean-Philippe Jais, Claudine Junien: C57BL/6J and

416 A/J mice fed a high-fat diet delineate components of metabolic syndrome. Obesity 2007, 15:1996-
417 2005.
418 [17] Patricia M. Watson SPC, Rudolph J. Beiler, Heather C. Hatcher, and Thomas W. Gettys:
419 Differential regulation of leptin expression and function in A/J vs. C57BL/6J mice during diet-
420 induced obesity. Am J Physiol Endocrinol Metab 2000, 279:E356-65.
421 [18] Kondo H, Minegishi Y, Komine Y, Mori T, Matsumoto I, Abe K, Tokimitsu I, Hase T, Murase
422 T: Differential regulation of intestinal lipid metabolism-related genes in obesity-resistant A/J vs.
423 obesity-prone C57BL/6J mice. Am J Physiol Endocrinol Metab 2006, 291:E1092-9.
424 [19] Ganz M: High fat diet feeding results in gender specific steatohepatitis and inflammasome
425 activation. World J Gastroenterol 2014, 20:8525.
426 [20] Norheim F, Hui ST, Kulahcioglu E, Mehrabian M, Cantor RM, Pan C, Parks BW, Lusis AJ:
427 Genetic and hormonal control of hepatic steatosis in female and male mice. J Lipid Res 2017,
428 58:178-87.
429 [21] Ichimura-Shimizu M, Omagari K, Yamashita M, Tsuneyama K: Development of a novel
430 mouse model of diet-induced nonalcoholic steatohepatitis-related progressive bridging fibrosis.
431 Biosci Biotechnol Biochem 2021, 85:941-7.
432 [22] Kleiner DE, Brunt EM, Van Natta M, Behling C, Contos MJ, Cummings OW, Ferrell LD,
433 Liu Y-C, Torbenson MS, Unalp-Arida A, Yeh M, McCullough AJ, Sanyal AJ: Design and
434 validation of a histological scoring system for nonalcoholic fatty liver disease. Hepatology 2005,
435 41:1313-21.

436 [23] Ioannou GN, Subramanian S, Chait A, Haigh WG, Yeh MM, Farrell GC, Lee SP, Savard C:
437 Cholesterol crystallization within hepatocyte lipid droplets and its role in murine NASH. J Lipid
438 Res 2017, 58:1067-79.
439 [24] Tsuneyama K, Nishitsuji K, Matsumoto M, Kobayashi T, Morimoto Y, Tsunematsu T, Ogawa
440 H: Animal models for analyzing metabolic syndrome-associated liver diseases. Pathol Int 2017,
441 67:539-46.
442 [25] Remmerie A, Scott CL: Macrophages and lipid metabolism. Cell Immunol 2018, 330:27-42.
443 [26] Ioannou GN, Landis CS, Jin GY, Haigh WG, Farrell GC, Kuver R, Lee SP, Savard C:
444 Cholesterol Crystals in Hepatocyte Lipid Droplets Are Strongly Associated With Human
445 Nonalcoholic Steatohepatitis. Hepatology Communications 2019, 3:776-91.
446 [27] Nidorf SM, Fiolet A, Abela GS: Viewing atherosclerosis through a crystal lens: How the
447 evolving structure of cholesterol crystals in atherosclerotic plaque alters its stability. J Clin Lipidol
448 2020, 14:619-30.
449 [28] Oishi Y, Spann NJ, Link VM, Muse ED, Strid T, Edillor C, Kolar MJ, Matsuzaka T,
450 Hayakawa S, Tao J, Kaikkonen MU, Carlin AF, Lam MT, Manabe I, Shimano H, Saghatelian A,
451 Glass CK: SREBP1 Contributes to Resolution of Pro-inflammatory TLR4 Signaling by
452 Reprogramming Fatty Acid Metabolism. Cell Metab 2017, 25:412-27.
453 [29] Lee J-H, Phelan P, Shin M, Oh B-C, Han X, Im S-S, Osborne TF: SREBP-1a–stimulated
454 lipid synthesis is required for macrophage phagocytosis downstream of TLR4-directed mTORC1.
455 PNAS 2018, 115:E12228-E34.

456 [30] Drasdo D, Hoehme S, Hengstler JG: How predictive quantitative modelling of tissue
457 organisation can inform liver disease pathogenesis. J Hepatol 2014, 61:951-6.
458 [31] Machado MV, Michelotti GA, Pereira TA, Xie G, Premont R, Cortez-Pinto H, Diehl AM:
459 Accumulation of duct cells with activated YAP parallels fibrosis progression in non-alcoholic
460 fatty liver disease. J Hepatol 2015, 63:962-70.
461 [32] Subramanian S, Goodspeed L, Wang S, Kim J, Zeng L, Ioannou GN, Haigh WG, Yeh MM,
462 Kowdley KV, O'Brien KD, Pennathur S, Chait A: Dietary cholesterol exacerbates hepatic steatosis
463 and inflammation in obese LDL receptor-deficient mice. J Lipid Res 2011, 52:1626-35.
464 [33] Loomba R, Abraham M, Unalp A, Wilson L, Lavine J, Doo E, Bass NM: Association between
465 diabetes, family history of diabetes, and risk of nonalcoholic steatohepatitis and fibrosis.
466 Hepatology 2012, 56:943-51.
467 [34] Angulo P, Hui JM, Marchesini G, Bugianesi E, George J, Farrell GC, Enders F, Saksena S,
468 Burt AD, Bida JP, Lindor K, Sanderson SO, Lenzi M, Adams LA, Kench J, Therneau TM, Day
469 CP: The NAFLD fibrosis score: A noninvasive system that identifies liver fibrosis in patients with
470 NAFLD. Hepatology 2007, 45:846-54.
471 [35] Puri P, Baillie RA, Wiest MM, Mirshahi F, Choudhury J, Cheung O, Sargeant C, Contos MJ,
472 Sanyal AJ: A lipidomic analysis of nonalcoholic fatty liver disease. Hepatology 2007, 46:1081-
473 90.
474 [36] Arguello G, Balboa E, Arrese M, Zanlungo S: Recent insights on the role of cholesterol in
475 non-alcoholic fatty liver disease. Biochimica et Biophysica Acta (BBA) - Molecular Basis of

476 Disease 2015, 1852:1765-78.

477 [37] Charlton M, Sreekumar R, Rasmussen D, Lindor K, Nair KS: Apolipoprotein synthesis in

478 nonalcoholic steatohepatitis. Hepatology 2002, 35:898-904.

479 [38] Farrell GC, Mridha AR, Yeh MM, Arsov T, Van Rooyen DM, Brooling J, Nguyen T, Heydet

480 D, Delghingaro-Augusto V, Nolan CJ, Shackel NA, McLennan SV, Teoh NC, Larter CZ: Strain

481 dependence of diet-induced NASH and liver fibrosis in obese mice is linked to diabetes and

482 inflammatory phenotype. Liver Int 2014, 34:1084-93.

483 [39] Ikemoto S, Takahashi M, Tsunoda N, Maruyama K, Itakura H, Kawanaka K, Tabata I,

484 Higuchi M, Tange T, Tokuo T, Yamamoto T, Ezaki O: Cholate inhibits high-fat diet-induced

485 hyperglycemia and obesity with acyl-CoA synthetase mRNA decrease. Am J Physiol 1997, 273:

486 E37-E45.

487 [40] Van Rooyen DM, Larter CZ, Haigh WG, Yeh MM, Ioannou G, Kuver R, Lee SP, Teoh NC,

488 Farrell GC: Hepatic Free Cholesterol Accumulates in Obese, Diabetic Mice and Causes

489 Nonalcoholic Steatohepatitis. Gastroenterology 2011, 141:1393-403.e5.

490 [41] Ioannou GN, Morrow OB, Connole ML, Lee SP: Association between dietary nutrient

491 composition and the incidence of cirrhosis or liver cancer in the United states population.

492 Hepatology 2009, 50:175-84.

493 [42] Fukuda A, Sasao M, Asakawa E, Narita S, Hisano M, Suruga K, Ichimura M, Tsuneyama K,

494 Tanaka K, Omagari K: Dietary fat, cholesterol, and cholic acid affect the histopathologic severity

495 of nonalcoholic steatohepatitis in Sprague-Dawley rats. Pathology - Research and Practice 2019,

496 215:152599.

497 [43] Yasutake K, Nakamuta M, Shima Y, Ohyama A, Masuda K, Haruta N, Fujino T, Aoyagi Y,

498 Fukuizumi K, Yoshimoto T, Takemoto R, Miyahara T, Harada N, Hayata F, Nakashima M,

499 Enjoji M: Nutritional investigation of non-obese patients with non-alcoholic fatty liver disease:

500 the significance of dietary cholesterol. Scand J Gastroenterol 2009, 44:471-7.

501 [44] Younes R, Bugianesi E: NASH in Lean Individuals. Semin Liver Dis 2019, 39:086-95.

502

503 **Figure legends**

504 Figure 1

505 Levels of hepatic and serum lipids and a liver injury markers in C57BL6/J and A/J mice fed the
506 normal, LC and HC diets for 9 weeks. Triglyceride (TG) levels of the liver (A) and serum (B). C:
507 TG levels in very low density lipoprotein (VLDL). D: Apolipoprotein B (ApoB) mRNA levels.
508 Total-cholesterol levels of the liver (E) and serum (F). G: Serum concentrations of ALT. Data are
509 expressed as means ± SE. n = 4 to 6 mice per group. *P<0.05, The significant strain × diet
510 interaction is detected by two-way ANOVA. †P<0.05, as determined by Tukey's test among the
511 3 diet groups in the same strain and by t-test between 2 strains fed with the same diet, respectively.
512 Strain × diet interactions were not significant. ALT, alanine aminotransferase; HC, high-
513 cholesterol; LC, low-cholesterol; T-chol, total cholesterol; TG, triglyceride.

514

515 Figure 2

516 Representative liver histopathology in C57BL6/J and A/J mice fed the normal, LC and HC diets
517 for 9 weeks. A: Hematoxylin and eosin (H&E)-, Oil red O- and Sirius red-stained sections; scale
518 bars = 200 μm. B: Positive area of Sirius red staining. Data are expressed as means ± SE. n = 4 to
519 6 mice per group. *P<0.05, as determined by Tukey's test among the 3 diet groups in the same
520 strain. Two-way ANOVA did not identify significant strain × diet interactions. C-K: Unique
521 structure of aggregated macrophages and ring-shaped fibrosis in the liver of A/J mice fed the HC
522 diet. H&E (C) and Sirius red (D) staining. Immunohistochemistry of collagen type I (E), IV (F),

523 Mac-2 (G), CD204 (H), MCP-1 (J), and PDGF-Rβ (K). Polarized light microscopy (I). Insets
524 show higher magnification images of ring-shaped fibrosis and Maltese cross (D and I,
525 respectively). Panels G and K are serial sections. Panels C and I are the same section. Briefly,
526 after observation by polarized light microscopy, the same sections were stained with H&E and
527 the location of the Maltese cross was determined. Scale bars = 50 μm (C-K). CV, central vein (D
528 and F).

529

530 Figure 3

531 MALDI-MSI images and mass spectra in liver sections obtained from A/J mice fed the HC and
532 normal diets for identification of phospholipids.

533 A: Optical and mass spectrometry images of liver sections. B: Images of hematoxylin and eosin
534 (H&E) sections from adjacent sections. Dashed lines indicate the same region observed by
535 MALDI-MSI; black circles, the site of aggregated foamy macrophages; the inset shows a higher
536 magnification image of the dotted-line rectangle; arrows indicate aggregated foamy macrophages.
537 C and D: Product ion of *m/z* 772.462 after tandem MS analysis in positive-ion (C) and negative-
538 ion (D) mode. $[M+H]^+$, protonated molecule; $[M-H]^-$, deprotonated molecule; MS/MS, tandem
539 MS. Scale bars = 2 mm

540

541 Figure 4

542 Gene and protein expression in the liver of C57BL6/J and A/J mice fed the normal, LC and HC

543 diets for 9 weeks. The levels of mRNA and protein involved in fibrogenesis (A-C), inflammatory
544 response (D) and lipid metabolism (E-H) were analyzed by real-time PCR and western blotting
545 and are expressed relative to the B6-N group and to B-actin levels, respectively. Data are
546 expressed as means ± SE. *n* = 4 to 6 mice per group for mRNA and *n* = 4 mice per group for
547 protein expression. * $P<0.05$, A significant strain × diet interaction is detected by two-way
548 ANOVA. $^{\dagger}P<0.05$, as determined by Tukey's test among the 3 diet groups in the same strain. The
549 strain × diet interaction was not significant. Acsl1, long-chain acyl-CoA synthase 1; ApoB,
550 apolipoprotein B; ApoC3, apolipoprotein C3; Col1a1, procollagen type I, alpha 1; Col4a1,
551 procollagen type IV, alpha 1; Srebp-1c, sterol regulatory element-binding protein 1c; Tgf-β1,
552 transforming growth factor; Tnf-α, tumor necrosis factor-α
553
554 Figure 5
555 A proposed model showing interactions between macrophages and myofibroblasts during the
556 onset of fibrosis in a NASH model of HFCC diet-fed A/J strain mice. Macrophages phagocytose
557 excess lipids including cholesterol (yellow circles), aggregate, and then resemble a nest of
558 macrophages containing cholesterol crystals. Hepatic stellate cells migrate near the macrophage
559 nest and produce collagen fibers (wavy red lines) as myofibroblasts.
560

561 Table 1 Primer sequences used in real-time PCR analysis

	Forward primer	Reverse primer
Abcg5	5'-AACATACAAGAGATGCCCATTCC-3'	5'-GTTGGATCCACCACAAGTGAAG-3'
Abcg8	5'-TGCAATGCCCTCTACAACTCC-3'	5'-AGATCCATGCAGGCACTATCC-3'
Acsl1	5'-CTTAAATAGCATCGCAACCCG-3'	5'- GGTTCTCTATGCAGAATTCTCCTCC-3'
ApoC3	5'-AGCTACTCCAGGTAATGCCC-3'	5'-GCACCTACGTACCATGAGTC-3'
ApoB	5'-GTCTACTTCCACCCACAGTCCC-3'	5'-ATCTGGAAGCTGCCTCTTCTT-3
β-actin	5'-ATAACCCTGAAGTGCTCGACATC-3'	5'-GGGTACCCGATCTGCAGACA-3'
Col1a1	5'-GGAAGAGCGGAGAGTACTGG-3'	5'-CAGACGGCTGAGTAGGGAAC-3'
Col4a1	5'-AACTTCGCCTCCAGGAACG-3'	5'-CAAACCGCACACCTGCTAATG-3'
Cyp7a1	5'-TACAGAGTGCTGGCCAAGAG-3'	5'-ATGCTATCTAGTACTGGCAGGTTG-3'
Il-6	5'-TGAGAAAAGAGTTGTGCAATGG-3'	5'-TCCAGTTTGGTAGCATCCATCA-3'
Ldlr	5'-CCTATTGCACTGGTTGCCC-3'	5'-AATGTGGAGCTCGTCCTCTG-3'
p65	5'-CTCTGGCGAATGGCTTTACT-3'	5'-AGGGGAAACAGATCGTCCAT-3'

Srebp-1c	5'-ACAGTCCAGCCTTTGAGGATAG-3'	5'-GACACAGAAAGGCCAGTACACA-3'
Tgf-β1	5'-GCAACATGTGGAACTCTACCAGAA-3'	5'-GACGTCAAAAGACAGCCACTC-3'
Tnf-α	5'-CAGGCGGTGCCTATGTCTCA-3'	5'-GGCTACAGGCTTGTCACTCGAA-3'

Abcg, ATP-binding cassette transporter; Acsl1, long-chain acyl-CoA synthase 1; ApoB, apolipoprotein B; ApoC3, apolipoprotein C3; Col1a1, procollagen type I, alpha 1; Col4a1, procollagen type IV, alpha 1; Cyp7a1, cytochrome P450 7A1; HmgCoAr, 3-hydroxy-3-methylglutaryl coenzyme A reductase; Il-6, interleukin-6; Ldlr, low-density lipoprotein receptor; Srebp-1c, sterol regulatory element-binding protein 1c; Tgf, transforming growth factor; Tnf-α, tumor necrosis factor-α

566 Table 2 Cumulative energy intake, body weight and organ weights of C57BL6/J and A/J mice fed the normal, LC and HC diets for 9 weeks.

Strain		**C57BL6/J**			**A/J**		
Diet type		Normal	LC	HC	Normal	LC	HC
Final BW	(g)	27.4 ± 0.8	27.8 ± 0.6	26.9 ± 0.6	26.1 ± 0.8	24.6 ± 0.3†	26.4 ± 0.7
BW gain	(%)	11.9 ± 2.8	13.1 ± 4.3	10.7 ± 2.8	23.6 ± 8.6	13.9 ± 2.5	20.3 ± 5.0
Cumulative energy intake	(kcal)	920 ± 23	940 ± 68	948 ± 35	908 ± 16	917 ± 32	832 ± 19
Liver weight/BW	(%)	5.03 ± 0.59	6.84 ± 0.46	7.42 ± 0.48*	4.81 ± 0.20‡	9.20 ± 0.68 *†§	8.85 ± 0.42 *†§
Epididymal fat pad weight/BW	(%)	1.68 ± 0.20	1.40 ± 0.08	1.32 ± 0.04	1.69 ± 0.38	0.98 ± 0.19	1.39 ± 0.23
Spleen weight/BW	(%)	0.26 ± 0.01	0.37 ± 0.03*§	0.41 ± 0.06*§	0.25 ± 0.02	0.40 ± 0.02*§	0.38 ± 0.04*§

567 Values are expressed as means ± SE. The significant strain × diet interaction is detected by two-way ANOVA in ratio of liver and spleen weight to BW.

568 The strain × diet interaction is not revealed in final BW but there is a significant difference between each LC groups, as determined by t-test between 2 strains fed with the

569 same diet. *P<0.05 vs. C57BL6/J-Normal; †P<0.05 vs. C57BL6/J-LC; ‡P<0.05 vs. C57BL6/J-HC; §P<0.05 vs. A/J- Normal. BW, body weight; LC, low-cholesterol; HC,

570 high-cholesterol.

571

572

573 Table 3 Serum parameters of C57BL6/J and A/J mice fed the normal, LC and HC diets for 9 weeks.

Strain		**C57BL6/J**			**A/J**		
Diet type		Normal	LC	HC	Normal	LC	HC
AST	(IU/L)	19.6 ± 2.4	41.3 ± 10.3	50.9 ± 3.9	45.0 ± 10.5	69.6 ± 25.2	73.9 ± 12.9
AST/ALT ratio		1.71 ± 0.49	1.66 ± 0.29	1.43 ± 0.12	3.23 ± 0.76	1.26 ± 0.13§	0.94 ± 0.15§
Glucose	(mg/ml)	193 ± 17	302 ± 57	177 ± 20	235 ± 50	271 ± 26	188 ± 14
Insulin	(ng/ml)	0.53 ± 0.16	0.36 ± 0.14	0.14 ± 0.02	0.30 ± 0.08	0.32 ± 0.15	0.10 ± 0.03
Leptin	(ng/ml)	1.14 ± 0.51	0.46 ± 0.14	0.17 ± 0.13	1.66 ± 0.94	0.87 ± 0.06	0.84 ± 0.04
LDL-C	(mg/dl)	6.6 ± 0.2	24.4 ± 2.5*	31.8 ± 3.5*	8.3 ± 0.5†‡	40.0 ± 3.2*†§	34.0 ± 2.5*§
HDL-C	(mg/dl)	47.7 ± 3.7	36.2 ± 1.8	43.9 ± 0.9	45.2 ± 1.6	42.2 ± 3.4	47.8 ± 4.5

574 Values are expressed as means ± SE. The significant strain × diet interaction is detected by two-way ANOVA in the AST/ALT ratio and LDL-C levels. *P<0.05 vs.

575 C57BL6/J-Normal; †P<0.05 vs. C57BL6/J-LC; ‡P<0.05 vs. C57BL6/J-HC; §P<0.05 vs. A/J- Normal. ALT, alanine aminotransferase; AST, aspartate aminotransferase; LC,

576 low-cholesterol; LDL-C, cholesterol in low density lipoprotein; HC, high-cholesterol; HDL-C, cholesterol in high density lipoprotein.

577

Table 4 Histopathological evaluation of the liver in C57BL6/J and A/J mice fed the normal, LC and HC diets for 9 weeks.

		C57BL6/J			A/J		
		Normal	LC	HC	Normal	LC	HC
Item/Group	Grade	(n=5)	(n=6)	(n=4)	(n=5)	(n=5)	(n=5)
Steatosis	0	5	2	0	5	0	0
	1	0	3	3	0	3	0
	2	0	1	1	0	2	5
Lobular inflammation	0	5	2	2	5	0	0
	1	0	2	1	0	1	1
	2	0	1	1	0	4	4
	3	0	1	0	0	0	0
Hepatocyte ballooning	0	5	2	1	5	0	0
	1	0	2	1	0	2	2
	2	0	2	2	0	3	3
NAFLD activity score (NAS)*	0-2	5	4	1	5	0	0
	3-4	0	0	2	0	1	1
	5-8	0	2	1	0	4	4
Fibrosis	0	5	0	1	5	0	0
	1	0	6	2	0	4	2
	2	0	0	1	0	1	3

*For the NAS, scores of 5 to 8 were considered to be diagnostic for NASH, and scores of 0 to 2 were considered to be not diagnostic for NASH. Values indicate the number of mice. LC, low-cholesterol; HC, high-cholesterol.

Fig1

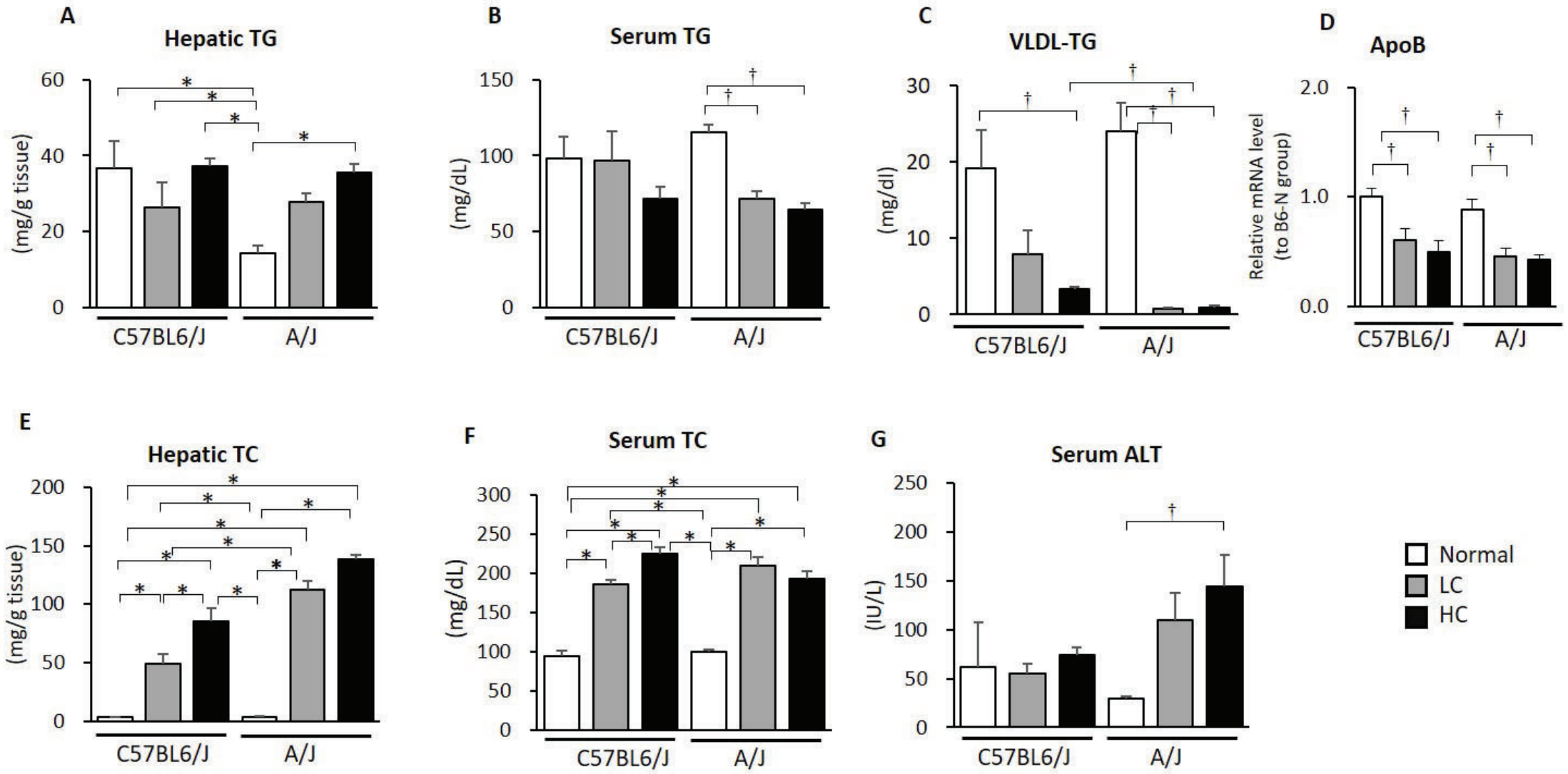
A
Hepatic TG
(mg/g tissue)
60
40
20
0
C57BL6/J
A/J
B
Serum TG
(mg/dL)
150
100
50
0
C57BL6/J
A/J
C
VLDL-TG
(mg/dl)
30
20
10
0
C57BL6/J
A/J
D
ApoB
Relative mRNA level
(to B6-N group)
2.0
1.0
0.0
C57BL6/J
A/J
E
Hepatic TC
(mg/g tissue)
200
150
100
50
0
C57BL6/J
A/J
F
Serum TC
(mg/dL)
300
250
200
150
100
50
0
C57BL6/J
A/J
G
Serum ALT
(IU/L)
250
200
150
100
50
0
C57BL6/J
A/J
Normal
LC
HC

Fig2

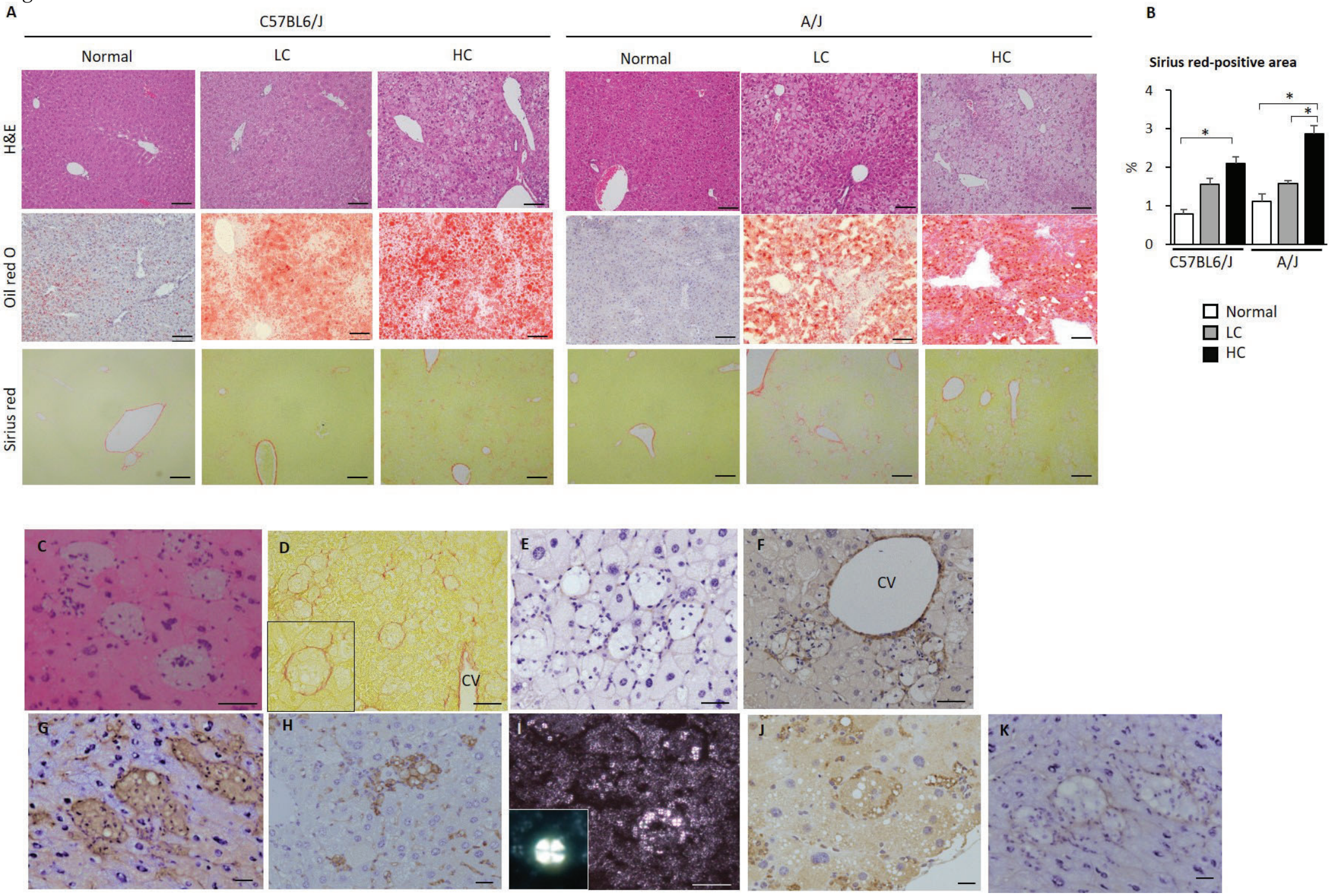
A
C57BL6/J
A/J
Normal
LC
HC
H&E
Oil red O
Sirius red
B
Sirius red-positive area
%
C57BL6/J
A/J
Normal
LC
HC
CV

Fig3

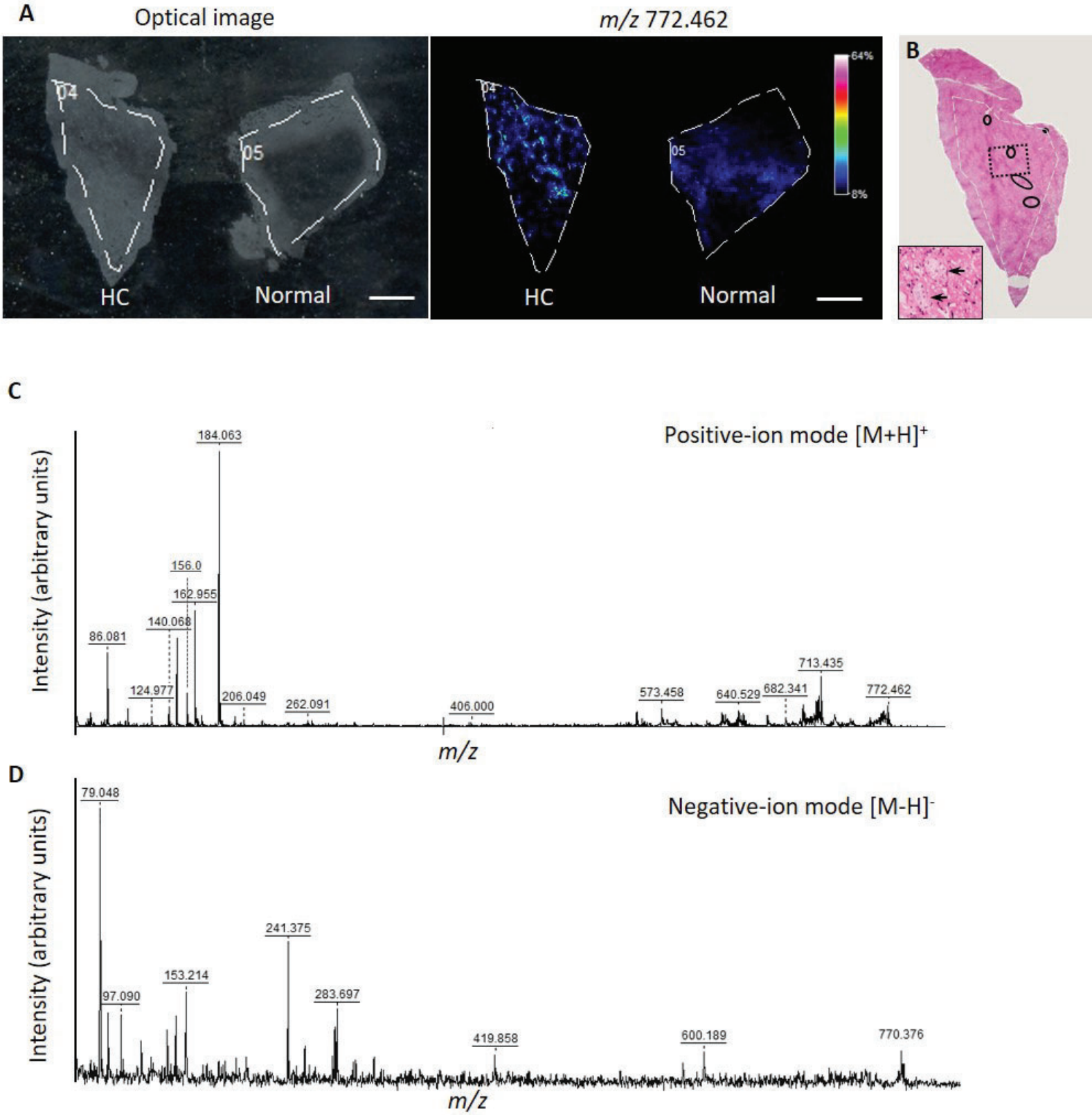
A
Optical image
m/z 772.462
04
05
HC
Normal
64%
8%
B
C
Positive-ion mode [M+H]+
Intensity (arbitrary units)
184.063
156.0
162.955
140.068
86.081
124.977
206.049
262.091
406.000
573.458
640.529
682.341
713.435
772.462
m/z
D
Negative-ion mode [M-H]-
79.048
241.375
153.214
97.090
283.697
419.858
600.189
770.376

Fig4

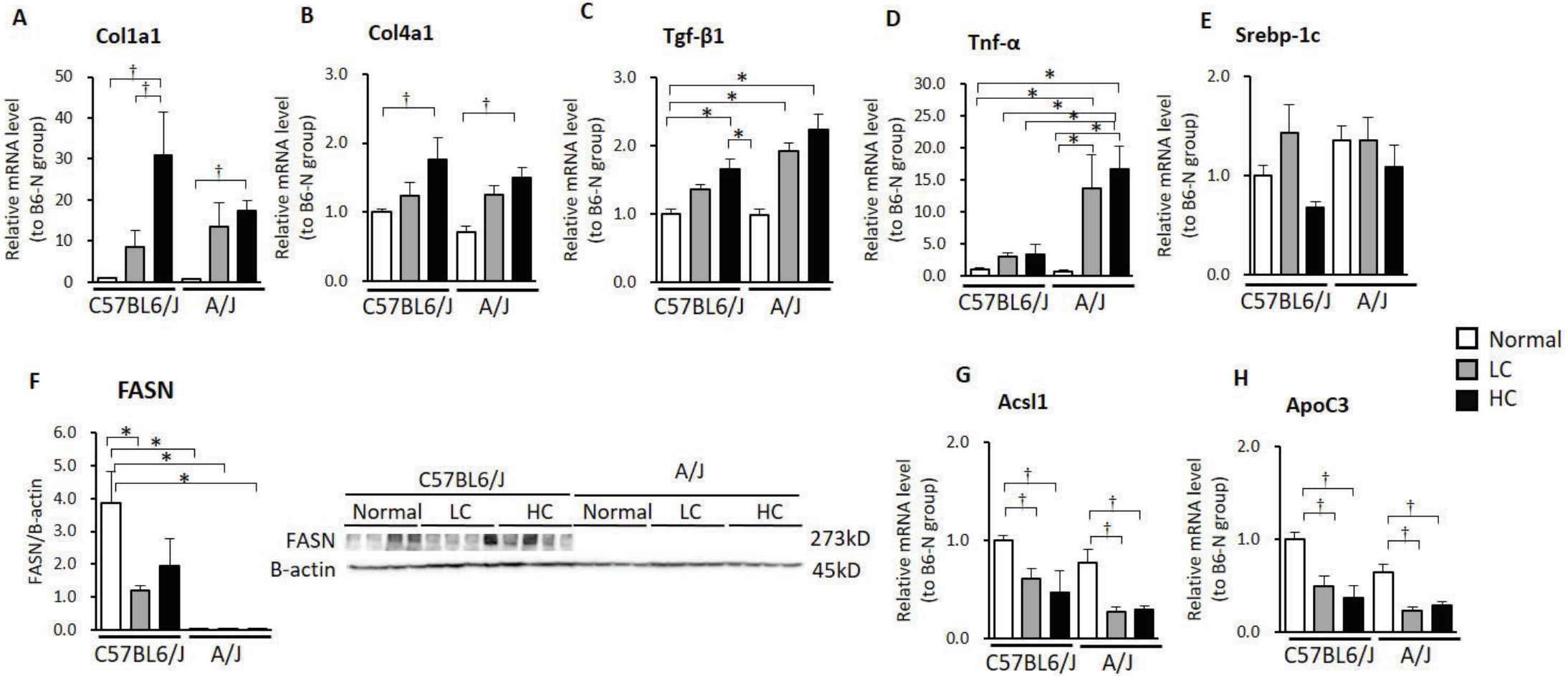
A
Col1a1
Relative mRNA level (to B6-N group)
C57BL6/J
A/J
B
Col4a1
C
Tgf-β1
D
Tnf-α
E
Srebp-1c
Normal
LC
HC
F
FASN
FASN/B-actin
C57BL6/J
A/J
Normal
LC
HC
FASN
B-actin
273kD
45kD
G
Acsl1
H
ApoC3

Fig5

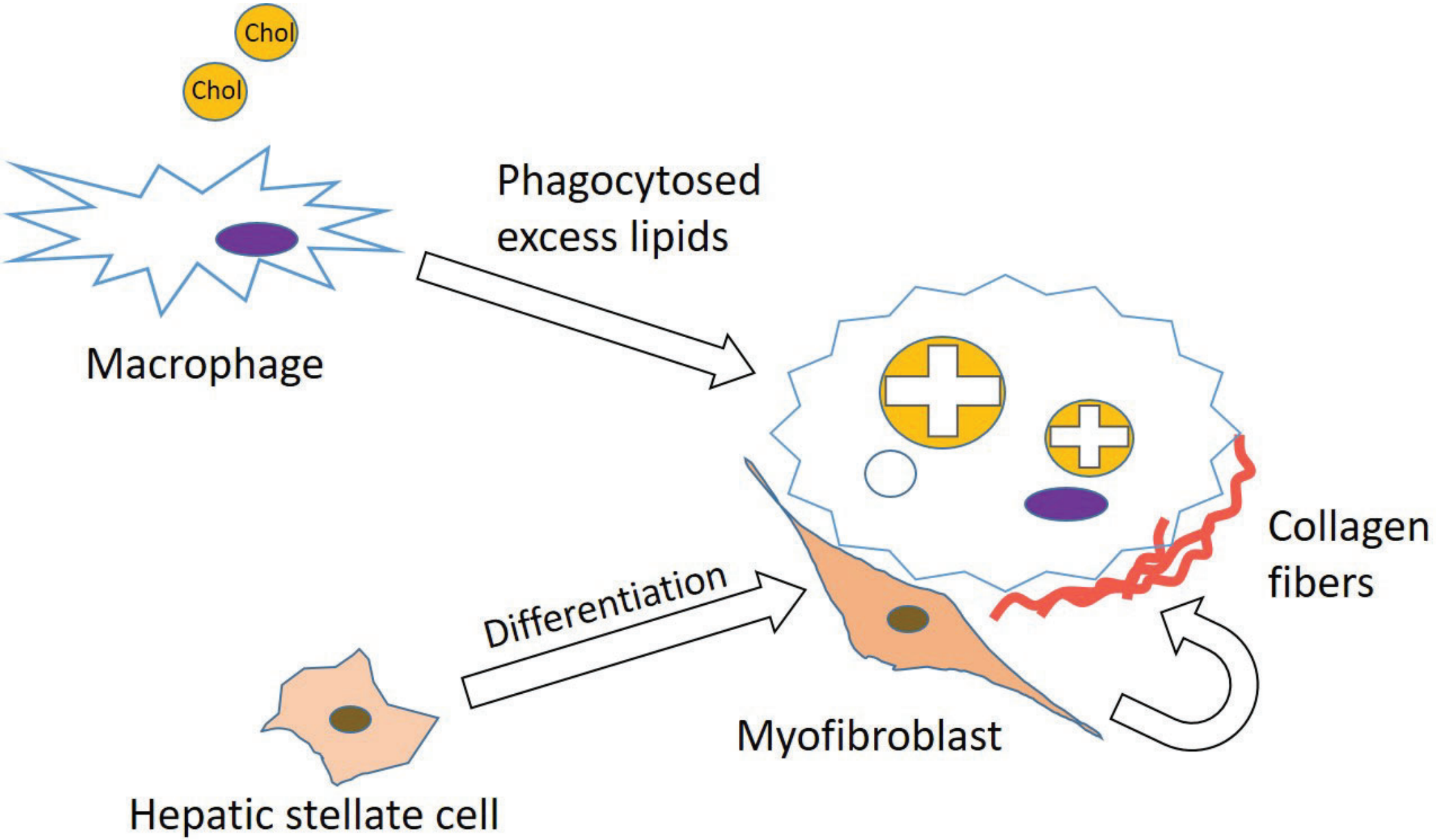
Chol
Chol
Macrophage
Phagocytosed
excess lipids
Differentiation
Hepatic stellate cell
Myofibroblast
Collagen
fibers

Supplemental figure legends

Supplemental Figure S1

Representative liver histopathology in C57BL6/J and A/J mice fed the normal and HC diets for 9 weeks. In the liver of C57BL6/J mice fed the HC diet, cholesterol crystals showing Maltese crosses were observed in the round white cells like lipid droplets in H&E staining. The arrows indicate same cells of the same liver section. The cholesterol crystals are surrounded by Mac-2- and CD204-positive macrophages, but differs from A/J mice in that there were few nest-like cluster of macrophages. Fibrosis is formed by linear fibers extending between hepatocytes (arrow heads), unlike the ring-shaped fibrosis seen in A/J mice. MCP-1 is positive not only around fibrotic lesions but also in some lymphocytes, although MCP-1 is a cytokine expressed by activated stellate cells. Scale bars = 50 μm. CV, central vein; P, portal tract; N.D., not detected.

Supplemental Figure S2

MALDI-MSI images of *m/z* 369.6 ion in liver sections from A/J mice fed the HC and normal diets. This molecular ion at *m/z* 369.6 was diffusely distributed in the liver section. Scale bars = 2 mm.

Supplemental Figure S3

Gene expression in the liver of C57BL6/J and A/J mice fed the normal, LC and HC diets for 9 weeks. The levels of mRNA involved in inflammation (A) and cholesterol metabolism (B) were measured by real-time PCR and are expressed relative to the B6-N group. Data are expressed as means ± SE. n = 4 to 6 mice per group. * $P<0.05$, A significant strain × diet interaction is detected by two-way ANOVA. †$P<0.05$, as determined by Tukey's test among the 3 diet groups in the same strain. The strain × diet interaction was not significant. Abcg, ATP-binding cassette

transporter; Cyp7a1, cytochrome P450 7A1; HmgCoAr, 3-hydroxy-3-methylglutaryl coenzyme A reductase; Il-6, interleukin-6; Ldlr, low-density lipoprotein receptor.

FigS1

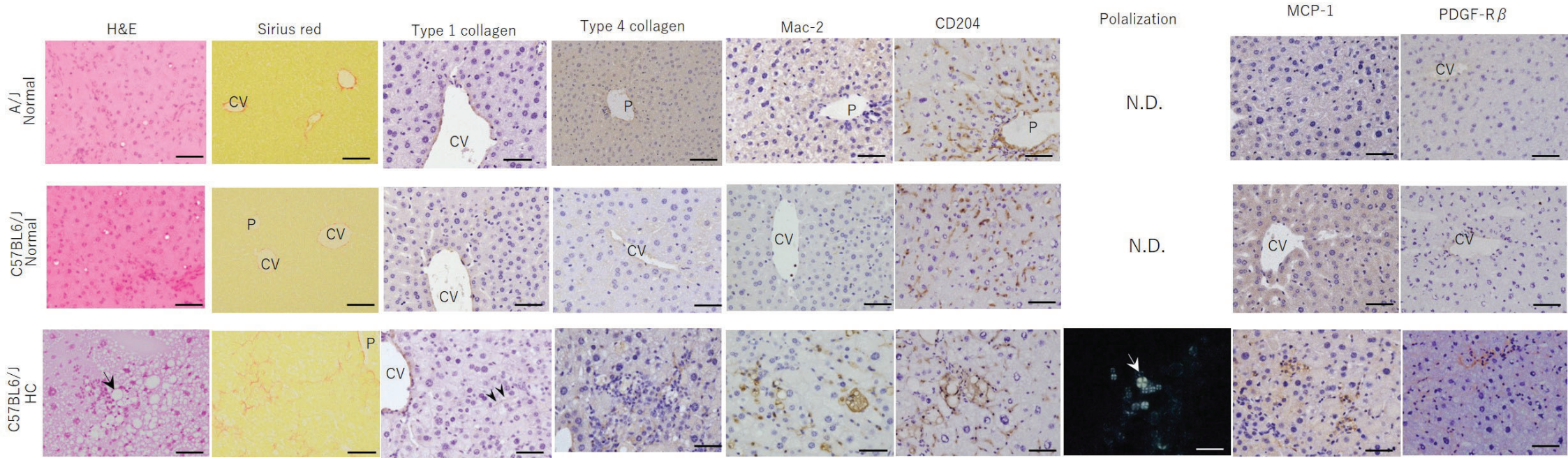
H&E
Sirius red
Type 1 collagen
Type 4 collagen
Mac-2
CD204
Polalization
MCP-1
PDGF-Rβ
A/J Normal
C57BL6/J Normal
C57BL6/J HC
CV
P
N.D.

FigS2

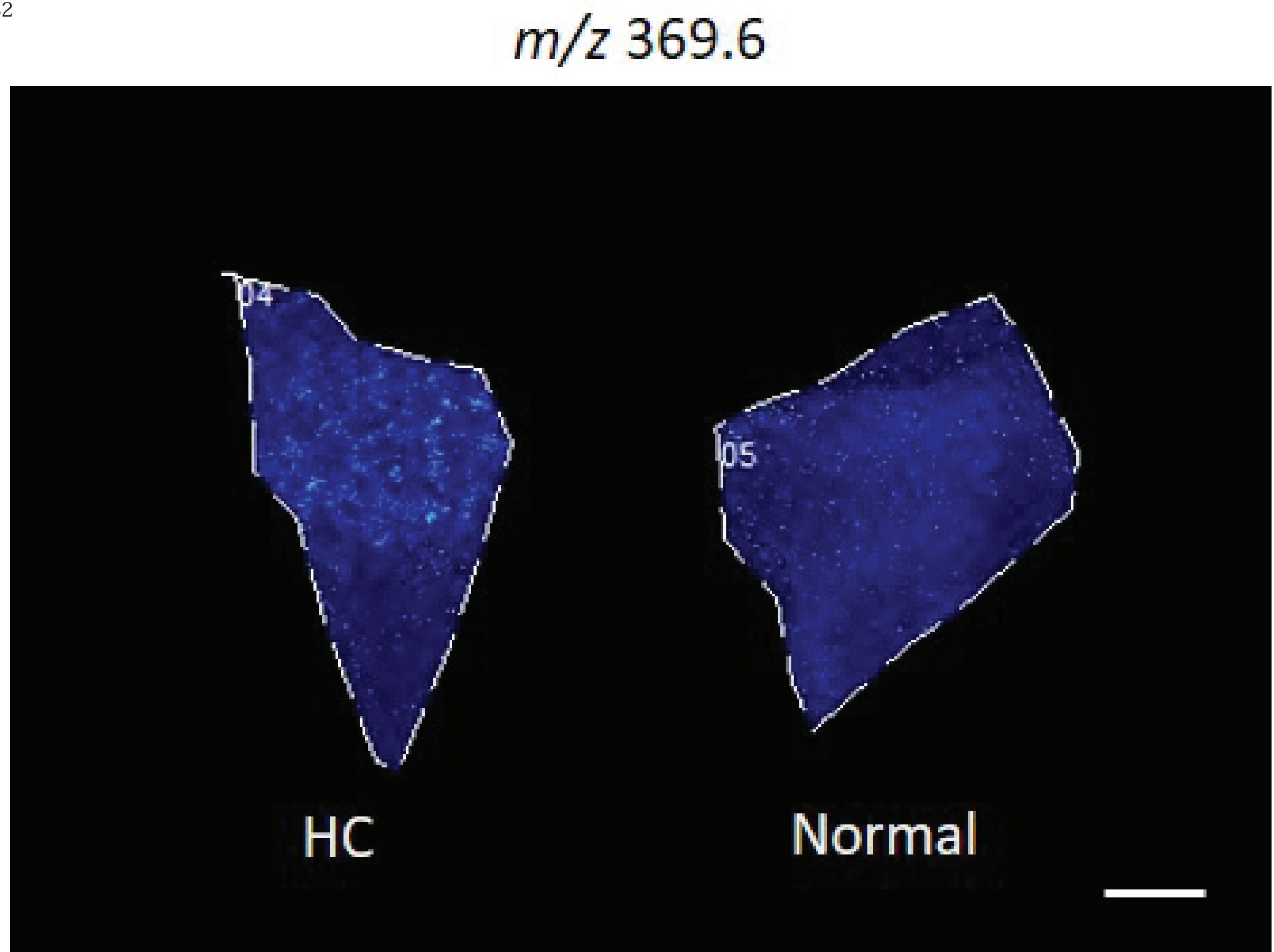

FigS3

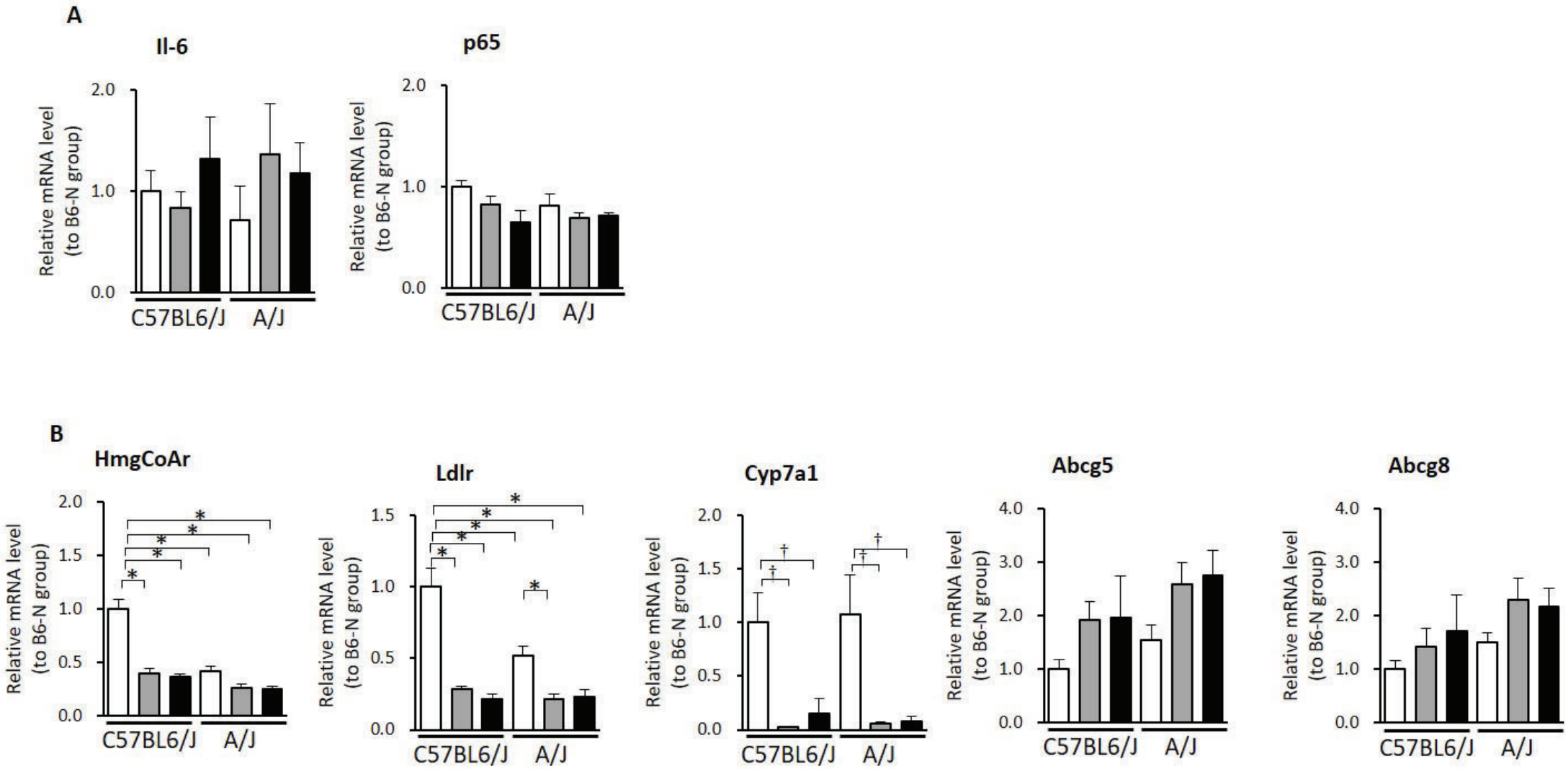
A
Il-6
p65
Relative mRNA level (to B6-N group)
2.0
1.0
0.0
C57BL6/J
A/J
B
HmgCoAr
Ldlr
Cyp7a1
Abcg5
Abcg8
1.5
0.5
3.0
4.0
*
†